universe

MDPI

Article

Properties of Heavy Higgs Bosons and Dark Matter Under Current Experimental Limits in the μNMSSM

Zhaoxia Heng [1], Xingjuan Li [2] and Liangliang Shang [1,3,*]

[1] School of Physics, Henan Normal University, Xinxiang 453007, China; zxheng@htu.edu.cn
[2] School of Physics and Electrical Engineering, Kashi University, Kashi 844006, China; lixingjuan@stu.htu.edu.cn
[3] Department of Physics and Astronomy, Uppsala University, P.O. Box 516, SE-751 20 Uppsala, Sweden
* Correspondence: shangliangliang@htu.edu.cn

Abstract: Searches for new particles beyond the Standard Model (SM) are an important task for the Large Hadron Collider (LHC). In this paper, we investigate the properties of the heavy non-SM Higgs bosons in the μ-term extended Next-to-Minimal Supersymmetric Standard Model (μNMSSM). We scan the parameter space of the μNMSSM considering the basic constraints from Higgs data, dark matter (DM) relic density, and LHC searches for sparticles. And we also consider the constraints from the LZ2022 experiment and the muon anomaly constraint at the 2σ level. We find that the LZ2022 experiment has a strict constraint on the parameter space of the μNMSSM, and the limits from the DM-nucleon spin-independent (SI) and spin-dependent (SD) cross-sections are complementary. Then, we discuss the exotic decay modes of heavy Higgs bosons decaying into SM-like Higgs bosons. We find that for doublet-dominated Higgs h_3 and A_2, the main exotic decay channels are $h_3 \to ZA_1$, $h_3 \to h_1h_2$, $A_2 \to A_1h_1$, and $A_2 \to Zh_2$, and the branching ratio can reach to about 23%, 10%, 35%, and 10% respectively.

Keywords: μNMSSM; heavy Higgs bosons; DM

check for updates

Academic Editor: Giuseppe Latino

Received: 19 December 2024
Revised: 5 March 2025
Accepted: 14 March 2025
Published: 20 March 2025

Citation: Heng, Z.; Li, X.; Shang, L. Properties of Heavy Higgs Bosons and Dark Matter Under Current Experimental Limits in the μNMSSM. *Universe* **2025**, *11*, 103. https://doi.org/10.3390/universe11030103

Copyright: © 2025 by the authors. Licensee MDPI, Basel, Switzerland. This article is an open access article distributed under the terms and conditions of the Creative Commons Attribution (CC BY) license (https://creativecommons.org/licenses/by/4.0/).

1. Introduction

In July 2012, both the ATLAS and CMS collaborations at the Large Hadron Collider (LHC) announced a scalar with mass near 125 GeV [1–3], and recently, the combined measurement of the muon anomalous magnetic moment by the Fermi National Accelerator Laboratory (FNAL) [4] and the Brookhaven National Laboratory (BNL) [5] showed a 4.2σ discrepancy from the prediction in the Standard Model (SM). The continuously updated experimental results provide rich information about supersymmetry (SUSY). As an economic realization of SUSY, the Next-to-Minimal Supersymmetric Standard Model (NMSSM) [6–10] has attracted more attention. However, considering the recent experimental constraints, the parameter space of the NMSSM with a discrete Z_3-symmetry (Z_3-NMSSM) has been strictly constrained [11–14]. In order to obtain a broad parameter space that agrees with the recent experimental results, we extend the Z_3-NMSSM by adding an explicit μ-term, which is called the μ-term extended NMSSM (μNMSSM) [14,15]. Compared with Z_3-NMSSM, the μNMSSM can easily explain the discrepancy of the muon anomalous magnetic moment in a broad parameter space while also coinciding with the experimental results in Dark Matter (DM) and Higgs physics, as well as the LHC searches for sparticles [12,16]. In addition, the μNMSSM is free from the tadpole problem and domain-wall problem in the Z_3-NMSSM. An extension of the MSSM called the $\mu\nu$SSM [17] is a model similar to the Z_3-NMSSM except that the singlet whose vacuum expectation

value (VEV) gives rise to the μ term also serves the role of a right-handed neutrino, thereby violating R-parity. Therefore, compared to the $\mu\nu$SSM, the μNMSSM can give a stable Lightest Supersymmetric Particle (LSP).

Since the discovery of a 125 GeV Standard Model (SM)-like Higgs boson at the LHC, the search for non-SM Higgs bosons has become even more pressing. In the μNMSSM, the lightest or next-to-lightest CP-even Higgs boson can be regarded as the SM-like Higgs boson. In addition to the SM-like Higgs boson (h_1 or h_2), the μNMSSM predicts another two CP-even neutral Higgs bosons (h_1/h_2 and h_3), two CP-odd neutral Higgs bosons (A_1 and A_2), and a pair of charged Higgs bosons ($H^{\pm}$). In this paper, we explore the discovery potential for the non-SM heavier Higgs bosons h_3 and A_2 in the μNMSSM at the LHC.

At present, besides the conventional search channels for heavy Higgs focusing on the decay modes into pairs of SM particles, the heavy Higgs exotic decay modes in the μNMSSM are kinematically open. The heavy neutral Higgs bosons can have a sizable branching ratio into two lighter neutral Higgs bosons, or into a lighter neutral Higgs boson and one Z boson. The relevant searches have been carried out at the LHC [18–25]. Ref. [26] has presented benchmark planes with cross-sections via gluon fusion for the exotic decay channels of heavy Higgs bosons in the NMSSM. And some discussions about the heavy Higgs exotic decays have also been conducted in the Two-Higgs-Doublet Model (2HDM) [27,28]. However, there have been no relevant discussions regarding the properties of the heavy Higgs boson in the μNMSSM. Therefore, our study aims to investigate the properties of the heavier CP-even Higgs boson h_3 and CP-odd Higgs boson A_2 in the μNMSSM. We focus on the searches for heavy Higgs bosons in final states with two lighter scalars, or one light scalar and a Z boson.

The outline of this paper is as follows: in Section 2, we briefly describe the relevant theoretical preliminaries of μNMSSM including the Higgs sector, the neutralino sector, and the DM-nucleon scattering cross-section. In Section 3, we give the numerical results considering the constraints of DM from the LZ experiment and investigate the properties of heavy Higgs bosons. In Section 4, we list the summary of this paper.

2. Theoretical Preliminaries

2.1. The Basics of the μNMSSM

To solve the problem in the Minimal Supersymmetric Standard Model (MSSM), such as the μ problem, the NMSSM is introduced. The NMSSM consisits of two Higgs doublet superfields, $\widehat{H}_u$ and $\widehat{H}_d$, and one singlet chiral superfield, $\widehat{S}$. After the electroweak symmetry breaking, the Higgs fields acquire the vacuum expected values (vevs); i.e., $< H_u >= v_u$, $< H_d >= v_d$, $< S >= v_s$, and $v = \sqrt{{v_u}^2 + {v_d}^2}$, $\tan\beta = \frac{v_u}{v_d}$. The Higgs fields in the NMSSM can be written as follows [10]:

$$\widehat{H}_u = \begin{pmatrix} H_u^+ \\ v_u + \frac{1}{\sqrt{2}}(\phi_u + i\varphi_u) \end{pmatrix}, \quad \widehat{H}_d = \begin{pmatrix} v_d + \frac{1}{\sqrt{2}}(\phi_d + i\varphi_d) \\ H_d^- \end{pmatrix}, \quad \widehat{S} = v_s + \frac{1}{\sqrt{2}}(\phi_s + i\varphi_s) \tag{1}$$

where ϕ_u, ϕ_d, and ϕ_s denote the neutral CP-even Higgs fields; φ_u, φ_d, and φ_s denote the neutral CP-odd Higgs fields; and H_u^+ and H_d^- denote the charged Higgs fields.

The general form of the superpotential in the NMSSM can be given by [10,29,30]

$$W_{\text{NMSSM}} = W_{\text{Yukawa}} + (\mu + \lambda\widehat{S})\widehat{H}_u \cdot \widehat{H}_d + \xi_F\widehat{S} + \frac{1}{2}\mu'\widehat{S}^2 + \frac{\kappa}{3}\widehat{S}^3 \tag{2}$$

where the term W_{Yukawa} is the same as that of the MSSM; μ and μ' are bilinear mass coefficients; λ and κ are dimensionless coupling coefficients; ξ_F is the supersymmetric

tadpole term of mass square dimension; and the parameters μ, μ', and ξ_F can be used to solve the tadpole problem and domain-wall problem in the Z_3-symmetry NMSSM [31–35].

In this work, we consider a specific scenario in which the parameters μ' and ξ_F in Equation (2) are equal to 0. This special scenario can be called the μ-term extended NMSSM (μNMSSM), which is more economical than GNMSSM in explaining the SM-like Higgs mass and the properties of DM. The superpotential and the corresponding soft breaking Lagrangian can be written as follows [33,34]:

$$W_{\mu\text{NMSSM}} = W_{\text{Yukawa}} + (\mu + \lambda\widehat{S})\widehat{H}_u \cdot \widehat{H}_d + \frac{\kappa}{3}\widehat{S}^3, \tag{3}$$

$$-\mathcal{L}_{\text{soft}} = \left[A_\lambda \lambda S H_u \cdot H_d + \frac{1}{3}A_\kappa \kappa S^3 + B_\mu \mu H_u \cdot H_d + h.c.\right] + m^2_{H_u}|H_u|^2 + m^2_{H_d}|H_d|^2 + m^2_S|S|^2, \tag{4}$$

where H_u, H_d, and S are the scalar parts of the superfields $\widehat{H}_u$, $\widehat{H}_d$, and $\widehat{S}$, respectively. By solving the minimization equation of the scalar potential, the soft breaking mass parameters $m^2_{H_u}$, $m^2_{H_d}$, and m^2_S can be expressed in terms of the vacuum expected values of the scalar field. To simplify the calculation, we set B_μ to be 0. Therefore, the Higgs sector is partially determined by the following parameters:

$$\tan\beta, \;\; \mu_{\text{eff}} = \lambda v_s/\sqrt{2}, \;\; \lambda, \;\; \kappa, \;\; A_\lambda, \;\; A_\kappa, \;\; \mu. \tag{5}$$

For convenience, we define $H_{\text{SM}} \equiv \sin\beta \text{Re}(H^0_u) + \cos\beta \text{Re}(H^0_d)$, $H_{\text{NSM}} \equiv \cos\beta \text{Re}(H^0_u) - \sin\beta \text{Re}(H^0_d)$, and $A_{\text{NSM}} \equiv \cos\beta \text{Im}(H^0_u) - \sin\beta \text{Im}(H^0_d)$, where H_{SM} is the SM Higgs field and its vev is $v/\sqrt{2}$, H_{NSM} is the other CP-even doublet Higgs field and its vev is zero, and A_{NSM} corresponds to the CP-odd Higgs boson in the MSSM [36,37]. In the basis $(H_{\text{NSM}}, H_{\text{SM}}, \text{Re}(S))$, the elements of the CP-even Higgs mass symmetric matrix M^2_S can be written as

$$\begin{aligned}
M^2_{S,11} &= \frac{2\mu_{eff}(\lambda A_\lambda + \kappa\mu_{eff})}{\lambda \sin 2\beta} + \frac{1}{2}(2m^2_Z - \lambda^2 v^2)\sin^2 2\beta, \\
M^2_{S,12} &= -\frac{1}{4}(2m^2_Z - \lambda^2 v^2)\sin 4\beta, \\
M^2_{S,13} &= -\frac{1}{\sqrt{2}}(\lambda A_\lambda + 2\kappa\mu_{eff})v\cos 2\beta, \\
M^2_{S,22} &= m^2_Z \cos^2 2\beta + \frac{1}{2}\lambda^2 v^2 \sin^2 2\beta, \\
M^2_{S,23} &= \frac{v}{\sqrt{2}}[2\lambda(\mu_{eff} + \mu) - (\lambda A_\lambda + 2\kappa\mu_{eff})\sin 2\beta], \\
M^2_{S,33} &= \frac{\lambda A_\lambda \sin 2\beta}{4\mu_{eff}}\lambda v^2 + \frac{\mu_{eff}}{\lambda}(\kappa A_\kappa + \frac{4\kappa^2\mu_{eff}}{\lambda}) - \frac{\mu}{2\mu_{eff}}\lambda^2 v^2.
\end{aligned} \tag{6}$$

And the elements of the CP-odd Higgs mass symmetric matrix M^2_P under the basis $(A_{NSM}, \text{Im}(S))$ is given by

$$\begin{aligned}
M^2_{P,11} &= \frac{2\mu_{eff}(\lambda A_\lambda + \kappa\mu_{eff})}{\lambda \sin 2\beta}, \\
M^2_{P,22} &= \frac{(\lambda A_\lambda + 4\kappa\mu_{eff})\sin 2\beta}{4\mu_{eff}}\lambda v^2 - \frac{3\kappa A_\kappa \mu_{eff}}{\lambda} - \frac{\mu}{2\mu_{eff}}\lambda^2 v^2, \\
M^2_{P,12} &= \frac{v}{\sqrt{2}}(\lambda A_\lambda - 2\kappa\mu_{eff}).
\end{aligned} \tag{7}$$

By diagonalizing M_S^2 and M_P^2 using the unitary matrix V and U, we can obtain the CP-even Higgs mass eigenstate $h_i(i = 1, 2, 3)$ with $m_{h_1} < m_{h_2} < m_{h_3}$, and CP-odd Higgs mass eigenstate $A_i(i = 1, 2)$ with $m_{A_1} < m_{A_2}$, respectively [34,38,39].

$$\begin{aligned} h_i &= V_{h_i}^{\mathrm{NSM}} H_{\mathrm{NSM}} + V_{h_i}^{\mathrm{SM}} H_{\mathrm{SM}} + V_{h_i}^{S} \mathrm{Re}(S), \\ A_i &= U_{A_i}^{\mathrm{NSM}} A_{\mathrm{NSM}} + U_{A_i}^{S} \mathrm{Im}(S). \end{aligned} \tag{8}$$

Each of the three CP-even Higgs bosons $h_i(i = 1, 2, 3)$ can be either SM-like (h), or H_{NSM} dominant (H), or singlet dominant (h_s). Likewise, each of the two CP-odd Higgs bosons A_i can be either singlet dominant (A_s), or H_{NSM} dominant (A_H).

The mass eigenstate of charged Higgs bosons is $H^{\pm} = \cos\beta H_u^{\pm} + \sin\beta H_d^{\pm}$, and their masses can be written as

$$m_{H^{\pm}}^2 = \frac{2\mu_{eff}(\lambda A_\lambda + \kappa \mu_{eff})}{\lambda \sin 2\beta} + m_W^2 - \lambda^2 v^2. \tag{9}$$

For neutralino sector, the neutralino mass eigenstate in the basis of $\psi^0 = \left(-i\tilde{B}^0, -i\tilde{W}^0, \tilde{H}_d^0, \tilde{H}_u^0, \tilde{S}^0\right)$ is

$$M_{\tilde{N}} = \begin{pmatrix} M_1 & 0 & -m_Z \sin\theta_{\mathrm{w}} \cos\beta & m_Z \sin\theta_{\mathrm{w}} \sin\beta & 0 \\ 0 & M_2 & m_Z \cos\theta_{\mathrm{w}} \cos\beta & -m_Z \cos\theta_{\mathrm{w}} \sin\beta & 0 \\ -m_Z \sin\theta_{\mathrm{w}} \cos\beta & m_Z \cos\theta_{\mathrm{w}} \cos\beta & 0 & -\mu_{\mathrm{tot}} & -\frac{1}{\sqrt{2}}\lambda v \sin\beta \\ m_Z \sin\theta_{\mathrm{w}} \sin\beta & -m_Z \cos\theta_{\mathrm{w}} \sin\beta & -\mu_{\mathrm{tot}} & 0 & -\frac{1}{\sqrt{2}}\lambda v \cos\beta \\ 0 & 0 & -\frac{1}{\sqrt{2}}\lambda v \sin\beta & -\frac{1}{\sqrt{2}}\lambda v \cos\beta & 2\frac{\kappa}{\lambda}\mu_{\mathrm{eff}} \end{pmatrix}, \tag{10}$$

where $\mu_{\mathrm{tot}} \equiv \mu + \mu_{\mathrm{eff}}$, and M_1 and M_2 are Bino and Wino soft breaking masses, respectively. After diagonalizing the mass matrix $M_{\tilde{N}}$ by rotation matrix N, we can obtain the neutralino mass eigenstate $\tilde{\chi}_i^0$ (i = 1, 2, 3, 4, 5) labeled in mass-ascending order, which can be expressed as

$$\tilde{\chi}_i^0 = N_{ij}\psi_j^0 (j = 1, 2, 3, 4, 5). \tag{11}$$

Assuming the lightest neutralino $\tilde{\chi}_1^0$ is the LSP, which can be considered as an ideal candidate for DM. Evidently, N_{11}^2, N_{12}^2, $N_{13}^2 + N_{14}^2$ and N_{15}^2 denote the Bino, Wino, Higgsino, and Singlino fractions in $\tilde{\chi}_1^0$, respectively. Different from the case in the Z_3-NMSSM, $2|\kappa|$ may be much larger than λ in obtaining Singlino-dominated DM.

2.2. The Heavy Higgs Bosons

In this work we require the lightest CP-even Higgs boson h_1 is SM-like, and investigate the properties of the heavy Higgs bosons h_3 and A_2. At the LHC, the heavy Higgs boson H (h_3 or A_2) is mainly produced through gluon-gluon fusion (ggF), and the production cross-section can be obtained by

$$\frac{\sigma(ggF \to H)}{\sigma(ggF \to h_{SM})} = \left| C_{ggF}^{H} \right|^2, \tag{12}$$

where h_{SM} denotes the SM-like Higgs boson, and C_{ggF}^{H} is the reduced coupling coefficient relative to the prediction in the SM. In the μNMSSM, the exotic decay modes of heavy Higgs bosons are open and heavy Higgs bosons h_3 and A_2 can have sizable branching ratio into two lighter Higgs bosons, e.g., $h_3 \to h_1 h_2$, $A_2 \to A_1 h_1$, which can be called Higgs-to-Higgs decays. In addition, heavy Higgs bosons h_3 and A_2 may decay into one light Higgs boson and a Z boson, e.g., $h_3 \to A_1 Z$, $A_2 \to h_1 Z$. The branching ratio of the Higgs-to-Higgs decays depends on trilinear Higgs couplings. For the typical case with

v_s, $A_\lambda \gg v_u, v_d \approx M_Z$, the relevant trilinear Higgs couplings relative to Higgs-to-Higgs decays can be expressed by (neglecting contributions of $\mathcal{O}(M_Z)$) [10,26] the following:

$$\begin{aligned}(1)H_{\rm NSM}H_{\rm SM}{\rm Re}(S): &\quad -\frac{\lambda}{\sqrt{2}}(2\kappa v_s + A_\lambda),\\ (2)A_{\rm NSM}H_{\rm SM}{\rm Im}(S): &\quad \sqrt{2}\lambda\sin\beta\cos\beta(-2\kappa v_s + A_\lambda).\end{aligned} \tag{13}$$

For the decays $h_i \to A_j + Z$ and $A_j \to h_i + Z$, the relevant couplings are

$$h_i(p)A_j(p')Z_\mu: \quad -igV_{h_i}^{\rm NSM}U_{A_i}^{\rm NSM}(p-p')_\mu \tag{14}$$

where $V_{h_i}^{\rm NSM}$ is the $H_{\rm NSM}$ component of the physical state h_i; and $U_{A_i}^{\rm NSM}$ is the $A_{\rm NSM}$ component of the physical state A_j.

2.3. The Anomalous Magnetic Moment of the Muon in the μNMSSM

The recent measurement of the muon anomalous magnetic moment a_μ^{exp} by the FNAL has been updated, and its value is [4]

$$a_\mu^{exp}({\rm FNAL}) = 116592040(54)\times 10^{-11}. \tag{15}$$

The result $a_\mu^{exp}({\rm FNAL})$ is in full agreement with the BNL E821 result $a_\mu^{exp}({\rm BNL})$ [5]:

$$a_\mu^{exp}({\rm BNL}) = 116592080(63)\times 10^{-11}. \tag{16}$$

And the combined experimental average a_μ^{exp} is [40–57]

$$a_\mu^{exp} = 116592061(41)\times 10^{-11}. \tag{17}$$

The latest lattice calculations have led to a prediction that differs from the experimental result of a_μ by only 0.9σ [58]. While the current value for the anomaly, combining the latest Standard Model prediction [40] and the improved experimental result [59], is $\Delta a_\mu^{\rm exp} = (249 \pm 48)\times 10^{-11}$. In our analysis, we use the same value for the discrepancy between theory and experiment as used in ref. [60], namely, $\Delta a_\mu^{\rm exp} = (251 \pm 59)\times 10^{-11}$ [4], in order to make the comparison systematic.

In SUSY, the contributions to $a_\mu^{\rm SUSY}$ mainly originate from the loops mediated by a smuon and a neutralino or a chargino and a muon-type sneutrino [61–71]. In the μNMSSM, the one-loop contributions to $a_\mu^{\rm SUSY}$ can be written as [72]

$$\begin{aligned} a_\mu^{SUSY} &= a_\mu^{\tilde\chi^0\tilde\mu} + a_\mu^{\tilde\chi^\pm\tilde\nu},\\ a_\mu^{\tilde\chi^0\tilde\mu} &= \frac{m_\mu}{16\pi^2}\sum_{i,l}\left\{-\frac{m_\mu}{12m_{\tilde\mu_l}^2}\left(\left|n_{il}^{\rm L}\right|^2+\left|n_{il}^{\rm R}\right|^2\right)F_1^{\rm N}(x_{il}) + \frac{m_{\tilde\chi_i^0}}{3m_{\tilde\mu_l}^2}{\rm Re}\left(n_{il}^{\rm L}n_{il}^{\rm R}\right)F_2^{\rm N}(x_{il})\right\},\\ a_\mu^{\tilde\chi^\pm\tilde\nu} &= \frac{m_\mu}{16\pi^2}\sum_{k}\left\{\frac{m_\mu}{12m_{\tilde\nu_\mu}^2}\left(\left|c_k^{\rm L}\right|^2+\left|c_k^{\rm R}\right|^2\right)F_1^{\rm C}(x_k) + \frac{2m_{\tilde\chi_k^\pm}}{3m_{\tilde\nu_\mu}^2}{\rm Re}\left(c_k^{\rm L}c_k^{\rm R}\right)F_2^{\rm C}(x_k)\right\},\end{aligned} \tag{18}$$

where $i = 1,2,3,4,5$, $j = 1,2$, $l = 1,2$ represent the neutralino, chargino, and smuon index, respectively. And

$$\begin{aligned} n_{il}^{\rm L} &= \frac{1}{\sqrt{2}}(g_2N_{i2}+g_1N_{i1})X_{l1}^* - y_\mu N_{i3}X_{l2}^*, \quad n_{il}^{\rm R} = \sqrt{2}g_1N_{i1}X_{l2} + y_\mu N_{i3}X_{l1},\\ c_k^{\rm L} &= -g_2V_{k1}^{\rm c}, \quad c_k^{\rm R} = y_\mu U_{k2}^{\rm c}, \quad x_{il} = m_{\tilde\chi_i^0}^2/m_{\tilde\mu_l}^2, \quad x_k = m_{\tilde\chi_k^\pm}^2/m_{\tilde\nu_\mu}^2,\end{aligned} \tag{19}$$

where X denotes the smuon mass rotation matrices; and U^C and V^C denote the chargino mass rotation matrix. $F_1(x)$ and $F_2(x)$ are loop functions of the kinematic variables x_{il} and x_k, and their expressions are written as [73,74] follows:

$$\begin{aligned} F_1^N(x) &= \frac{2}{(1-x)^4}\Big[1-6x+3x^2+2x^3-6x^2\ln x\Big], \\ F_2^N(x) &= \frac{3}{(1-x)^3}\Big[1-x^2+2x\ln x\Big], \\ F_1^C(x) &= \frac{2}{(1-x)^4}\Big[2+3x-6x^2+x^3+6x\ln x\Big], \\ F_2^C(x) &= -\frac{3}{2(1-x)^3}\Big[3-4x+x^2+2\ln x\Big]. \end{aligned} \tag{20}$$

For the scenario with mass-degenerate sparticles, the relationship $F_1^N(1) = F_2^N(1) = F_1^C(1) = F_2^C(1) = 1$ holds.

2.4. DM-Nucleon Scattering Cross-Section

In the μNMSSM, the lightest neutralino $\tilde{\chi}_1^0$ as the LSP can be considered as a DM candidate [75,76]. The Higgsino fraction of $\tilde{\chi}_1^0$ plays an important role in elastic scattering between $\tilde{\chi}_1^0$ and nucleon. In the scenario with massive squarks, the Spin-Dependent (SD) scattering of $\tilde{\chi}_1^0$ with nucleons is mediated by exchanging a Z boson, and the scattering cross-section is approximated given by [77,78]

$$\sigma^{\mathrm{SD}}_{\tilde{\chi}_1^0-N} \simeq C_N \times \left(\frac{N_{13}^2 - N_{14}^2}{0.1}\right)^2, \tag{21}$$

where $N = p(n)$, denoting protons (neutrons), $C_p \simeq 4\times10^{-4}$ pb, $C_n \simeq 3.1$ pb, and

$$N_{13}^2 - N_{14}^2 = (\frac{\lambda v}{\sqrt{2}\mu_{tot}})^2 \frac{N_{15}^2\cos 2\beta}{1-(m_{\tilde{\chi}_1^0}/\mu_{tot})^2}. \tag{22}$$

The spin-independent (SI) scattering of $\tilde{\chi}_1^0$ with nucleons is mainly produced by exchanging CP-even Higgs bosons through the t-channel, and the cross-section is as follows [15,79,80]:

$$\sigma^{SI}_{\tilde{\chi}_1^0-N} = \frac{4\tilde{\mu}_R^2}{\pi}\left|f^{(N)}\right|^2, \tag{23}$$

where $\tilde{\mu}_R \equiv m_N m_{\tilde{\chi}_1^0}/(m_N + m_{\tilde{\chi}_1^0})$, denoting the reduced mass of the DM-nucleon system. The expressions of the effective couplings $f^{(N)}$ are

$$f^{(N)} = \sum_{h_i=h,H,h_S} f_{h_i}^{(N)} = \sum_{h_i=h,H,h_S} \frac{C_{\tilde{\chi}_1^0\tilde{\chi}_1^0 h_i} C_{NNh_i}}{2m_{h_i}^2}, \tag{24}$$

with C_{NNh_i} being the coupling coefficient between the CP-even Higgs bosons and nucleon,

$$C_{NNh_i} = -\frac{m_N}{v}\left[F_d^{(N)}(V_{h_i}^{\mathrm{SM}} - \tan\beta V_{h_i}^{\mathrm{NSM}}) + F_u^{(N)}\left(V_{h_i}^{\mathrm{SM}} + \frac{1}{\tan\beta}V_{h_i}^{\mathrm{NSM}}\right)\right], \tag{25}$$

where $F_d^{(N)} = f_d^{(N)} + f_s^{(N)} + \frac{2}{27}f_G^{(N)}$ and $F_u^{(N)} = f_u^{(N)} + \frac{4}{27}f_G^{(N)}$. The form factors $f_q^{(N)} = m_N^{-1}\langle N|m_q q\bar{q}|N\rangle$ $(q = u,d,s)$ denote the normalized light quarks contribution to the nucleon mass, and $f_G^{(N)} = 1 - \sum_{q=u,d,s} f_q^{(N)}$ represents other heavy quarks mass fraction in the nucleon.

3. Numerical Results

The parameter space of the μNMSSM has been scanned by EasyScan_HEP [81] with the Metropolis–Hastings algorithm:

$$\begin{gathered} |M_1| \leq 1.5 \text{ TeV}, \quad 100 \text{ GeV} \leq M_2 \leq 1.5 \text{ TeV}, \\ 0 \leq \lambda \leq 0.75, \quad |\kappa| \leq 0.75, \quad 1 \leq \tan\beta \leq 60, \quad 2 \text{ TeV} \leq |A_t| \leq 5 \text{ TeV}, \\ 10 \text{ GeV} \leq \mu \leq 1 \text{ TeV}, \quad 100 \text{ GeV} \leq \mu_{\text{tot}} \leq 1 \text{ TeV}, \quad |A_\kappa| \leq 700 \text{ GeV}, \\ 100 \text{ GeV} \leq m_{\tilde{\mu}_L} \leq 1 \text{ TeV}, \quad 100 \text{ GeV} \leq m_{\tilde{\mu}_E} \leq 1 \text{ TeV}. \end{gathered} \tag{26}$$

For other supersymmetric parameters, we fix them at 2 TeV. We use the package SARAH-4.14.3 [82–85] to generate the model files in the μNMSSM, use the program SPheno-4.0.4 [86,87] to obtain the particle spectrum, and use the package MicrOMEGAs-5.2.13 [88–97] to calculate the DM observables.

To be specific, we require the samples to satisfy the following basic constraints:

1. The lightest CP-even Higgs boson h_1 should be SM-like, and its mass should be between 121 GeV and 129 GeV. We utilize the code HiggsSignals-2.2.3 [98] to fit the properties of the SM-like Higgs boson to LHC Higgs data and utilize the code HiggsBounds-5.3.2 [99] to implement the constraints from the direct search for extra Higgs bosons at the LEP and Tevatron.

2. We assume the lightest neutralino is one of the DM candidates, so when comparing the dark matter scattering cross-section below with the experimental limit, we need the DM relic density $\Omega h^2 < 0.120$ [100]. The SI and SD DM cross-sections should be scaled by a factor $\Omega h^2/0.120$.

3. We consider the constraints from the direct detection experiments for sparticles at the LHC, and use SModelS-2.3.2 [101–104] to decompose the spectrum including these processes:

$$pp \to \tilde{\chi}_1^+ \tilde{\chi}_1^-, \; pp \to \tilde{\chi}_1^\pm \tilde{\chi}_{1,2,3}^0, \; pp \to \tilde{\mu}_L \tilde{\mu}_L^*, \; pp \to \tilde{\mu}_R \tilde{\mu}_R^*. \tag{27}$$

The Next-to-Leading Order (NLO) cross-sections of these processes at $\sqrt{s}$ = 13 TeV are calculated by Prospino2.1 [105]. In the following discussions, all the surviving samples satisfy these basic constraints.

3.1. Properties of Dark Matter

We project all the surviving samples from the scan onto a two-dimensional diagram, as shown below. The surviving samples are divided into three categories by three different colors: the purple samples satisfy the basic constraints mentioned above; the yellow samples satisfy not only the basic constraints but also the muon anomaly constraint within the 2σ level; and the red samples satisfy the basic constraints, the muon anomaly constraint within the 2σ level, and also the LZ experiment constraint in the year 2022 (LZ2022) [106].

Figure 1 shows the surviving samples on the plane $m_{\tilde{\chi}_1^0} - \sigma_p^{SI}$ and $m_{\tilde{\chi}_1^0} - \sigma_n^{SD}$. The green line on the left (right) plot is the upper limit of SI (SD) nucleon-DM cross-sections, which comes from the results of the recent LZ2022 experiment. The samples above the green line are excluded by the LZ2022 experiment. From this figure, we conclude that the results of recent nucleon-DM experiments impose strong constraints on the parameter space in the μNMSSM, and the SD limit is complementary to the SI limit in limiting the parameter space in the μNMSSM. The figure also reveals 100 GeV $\lesssim m_{\tilde{\chi}_1^0} \lesssim$ 400 GeV considering the constraints from the recent LZ2022 experiment.

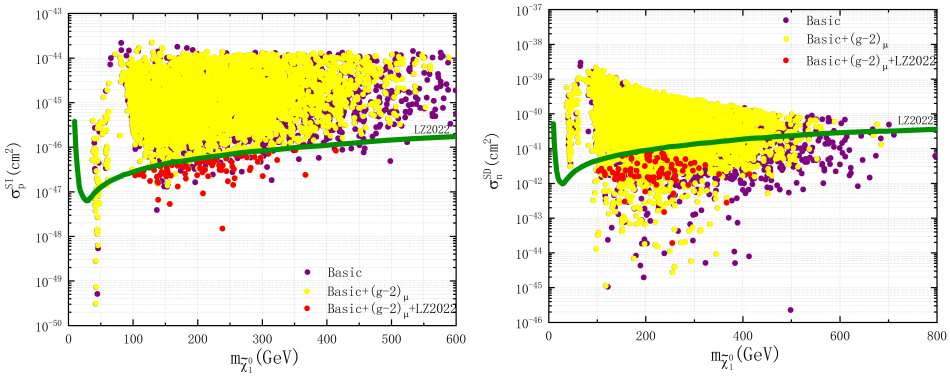


Figure 1. SI (**left plot**) and SD (**right plot**) nucleon-DM cross-section versus the mass of DM. The green lines stand for limits from LZ2022. Purple samples satisfy the basic constraints; yellow samples satisfy the anomaly of $(g-2)_\mu$ within the 2σ level further, and red samples satisfy the basic constraints, muon anomaly constraint within the 2σ level, and also the LZ2022 experiment constraint.

We display the characteristics of DM components in Figure 2. The upper left plot exhibits the Bino-component N_{11}^2, the upper right plot exhibits the Wino-component N_{12}^2, the lower left plot shows the Higgsino-component $N_{13}^2 + N_{14}^2$, and the lower right plot shows the Singlino-component N_{15}^2. Considering the constraints from the anomaly of $(g-2)_\mu$ and the recent LZ2022 experiment, the dark matter are mainly Wino-dominated or Higgsino-dominated. A few samples are Bino-dominated, but no samples are Singlino-dominated. The mass of Wino-dominated DM is less than 300 GeV, the mass of Higgsino-dominated DM is less than 350 GeV, and the mass of Bino-dominated DM is less than 400 GeV.

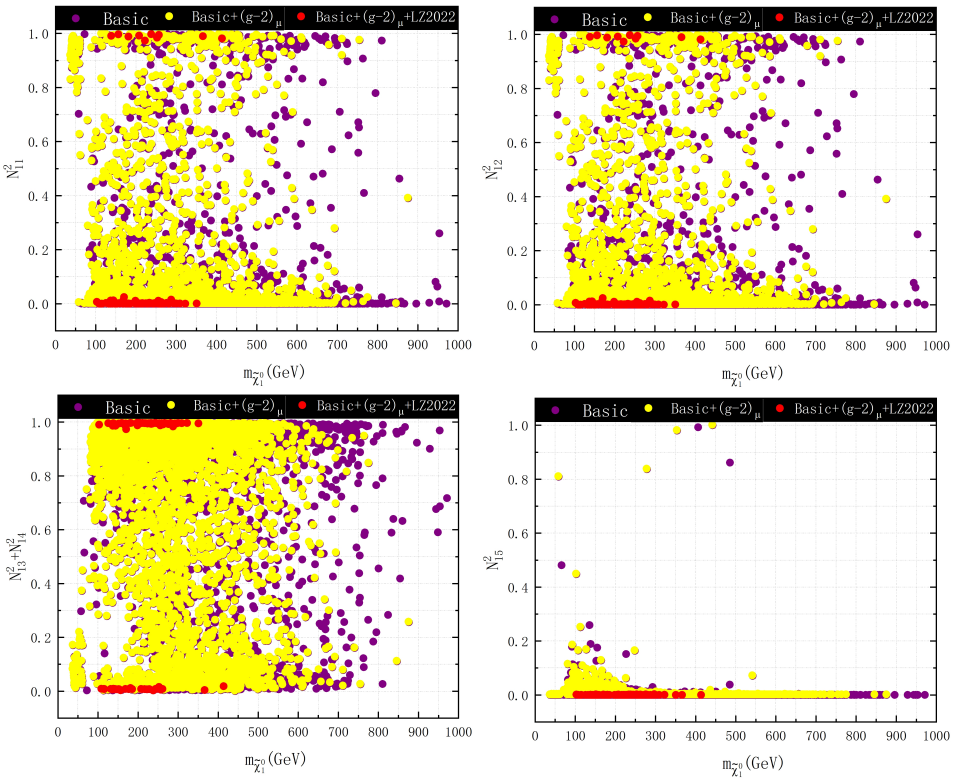


Figure 2. Similar with Figure 1, but shows the DM components versus the the mass of DM.

To investigate the properties of the surviving parameter space, we pick out the red samples in Figures 1 and 2 and project them onto $|\mu_{tot}/\mu_{eff}| - 2|\kappa|/\lambda$, $m_{\tilde{\chi}_1^0} - \tan\beta$, $M_2 - \mu_{tot}$ planes in Figure 3. For the Higgsino-dominated DM, $2|\kappa|/\lambda$ is much larger than $|\mu_{tot}/\mu_{eff}|$

as can be seen from the left plot, which is significantly different from the scenario in the Z_3-NMSSM. In the Z_3-NMSSM, Higgsino-dominated DM only requires $2|\kappa|/\lambda$ are larger than 1. The middle plot shows that $\tan\beta$ is greater than 20 for the Wino-dominated or Higgsino-dominated DM. From the right plot, we can see that the survival samples mainly tend to be 850 GeV $\lesssim M_2 \lesssim$ 1500 GeV and 100 GeV $\lesssim \mu_{\rm tot} \lesssim$ 300 GeV for Higgsino-dominated DM, and 100 GeV $\lesssim M_2 \lesssim$ 300 GeV and 800 GeV $\lesssim \mu_{\rm tot} \lesssim$ 1000 GeV for the Wino-dominated DM.

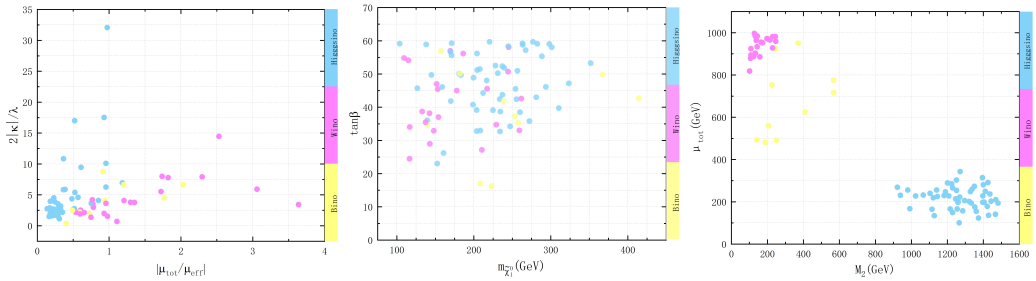


Figure 3. Survived samples projected onto $|\mu_{tot}/\mu_{eff}| - 2|\kappa|/\lambda$, $m_{\tilde{\chi}_1^0} - \tan\beta$ and $M_2 - \mu_{tot}$ planes. The yellow points denote the Bino-dominated DM, light purple points denote the Wino-dominated DM, and blue points denote the Higgsino-dominated DM.

3.2. Properties of Heavy Higgs Bosons

We pick out the survival samples satisfying the basic constraints mentioned above, and also the constraints from the anomaly of $(g-2)_\mu$ and the limit of SI (SD) nucleon-DM cross-sections to investigate the properties of heavy Higgs bosons h_3 and A_2. In Figure 4, we show the singlet component of the non-SM CP-even and CP-odd Higgs bosons. From the upper plots, we can see that for most of the survival samples, the next-to-lightest CP-even Higgs boson h_2 can be mostly singlet-dominated or doublet-dominated. Correspondingly, the heaviest CP-even Higgs boson h_3 can be mostly doublet-dominated or singlet-dominated. But for a portion of the samples, singlet-doublet mixing can be large. The lower plots show that for most of the surviving samples, the lightest CP-odd Higgs boson A_1 is mostly singlet-dominated and the heaviest CP-odd Higgs boson A_2 is mostly doublet-dominated. However, for a part of the samples, singlet-doublet mixing can be large. And for a small fraction of the samples, A_2 can be mostly singlet-dominated.

As discussed above, the exotic decay channels of heavy Higgs bosons h_3 and A_2 are open. In Figures 5 and 6 we show the exotic decay channels of h_3 and A_2, and we only consider the decay channels of heavy Higgs boson decaying into lighter Higgs boson. The left (right) plot of Figure 5 shows that h_3 is doublet-dominated (singlet-dominated), and the left (right) plot of Figure 6 shows A_2 is doublet-dominated (singlet-dominated). For the doublet-dominated Higgs boson h_3, the main decay channels are $h_3 \to ZA_1$ and $h_3 \to h_1h_2$, and the branching ratio can reach about 23% and 10%, respectively. The decay $h_3 \to ZA_1$ is proportional to the $A_{\rm NSM}$ component of the physical state A_1. The large branching ratio of $h_3 \to ZA_1$ just corresponds to the scenario that the doublet component of A_1 is relatively large. The decay $h_3 \to h_1h_2$ is proportional to the Higgs trilinear coupling shown in the first equation of Equation (13), which is usually relatively large when the mixing between doublet and singlet scalar fields is large. The singlet-dominated Higgs boson h_3 mainly decays into A_1A_1, and the branching ratio of $h_3 \to A_1A_1$ can reach to about 1.

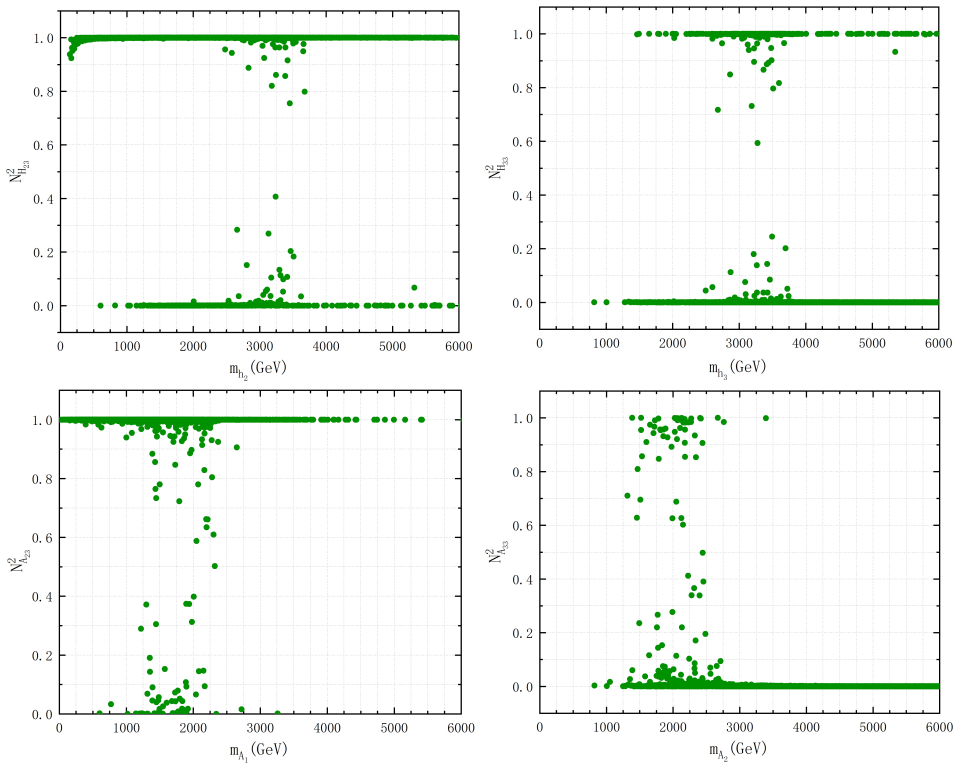


Figure 4. The singlet component of the non-SM CP-even and CP-odd Higgs bosons versus their masses.

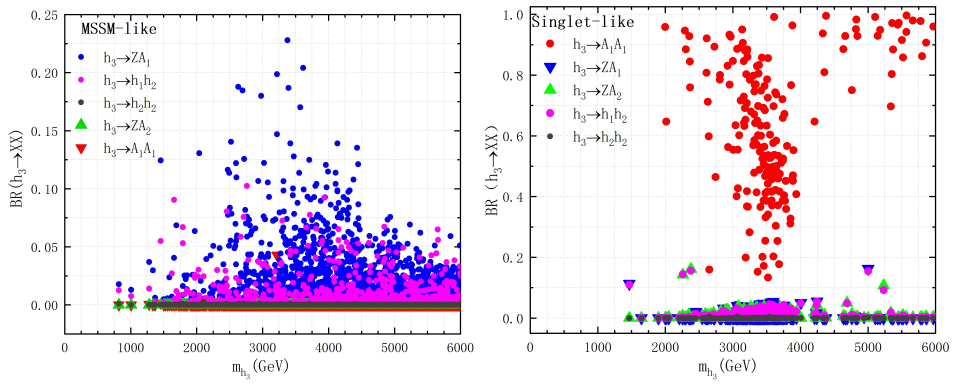


Figure 5. The exotic decay channels of the heavy CP-even Higgs boson h_3. The (**left plot**) denotes h_3 being doublet-dominated (MSSM-like), and the (**right plot**) denotes h_3 being singlet-dominated (singlet-like).

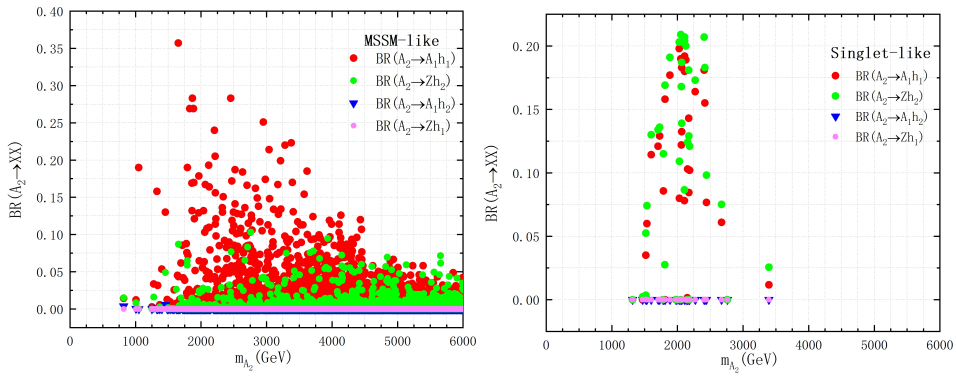


Figure 6. The exotic decay channels of heavy CP-odd Higgs boson A_2. The (**left plot**) denotes A_2 being doublet-dominated (MSSM-like), and the (**right plot**) denotes A_2 being singlet-dominated (singlet-like).

Figure 6 shows that for the doublet-dominated Higgs boson A_2, the main decay channels of the Higgs boson A_2 are $A_2 \to A_1 h_1$ and $A_2 \to Z h_2$, and the branching ratio can reach to about 35% and 10%, respectively. The decay $A_2 \to A_1 h_1$ is proportional to the Higgs trilinear coupling shown in the second equation of Equation (13), which is usually relatively large when the mixing between doublet and singlet pseudoscalar fields is large, as the off-diagonal element $M^2_{P,12}$ shown. The decay $A_2 \to Z h_2$ is proportional to the $H_{\rm NSM}$ component of the physical state h_2. The large branching ratio of $A_2 \to Z h_2$ just corresponds to the scenario that the doublet component of h_2 is relatively large. The branching ratio of the decay $A_2 \to Z h_1$ approaches 0 because the $H_{\rm NSM}$ component of the SM-like h_1 is much lower. The main decay channels of the singlet-dominated Higgs boson A_2 are $A_2 \to A_1 h_1$ and $A_2 \to Z h_2$.

Since the production cross-section of singlet-dominated Higgs bosons at the LHC is very small, we only consider the production of doublet-dominated Higgs bosons h_3 and A_2. In Figures 7 and 8, we show the production cross-section of the Higgs bosons h_3 and A_2 with h_3 and A_2 decaying into the SM-like Higgs at $\sqrt{s} = 13$ TeV LHC. We find that the cross-sections $ggF \to h_3 \to h_1 h_2$ and $ggF \to A_2 \to A_1 h_1$ can reach to about 10^{-11} pb and 10^{-10} pb, respectively.

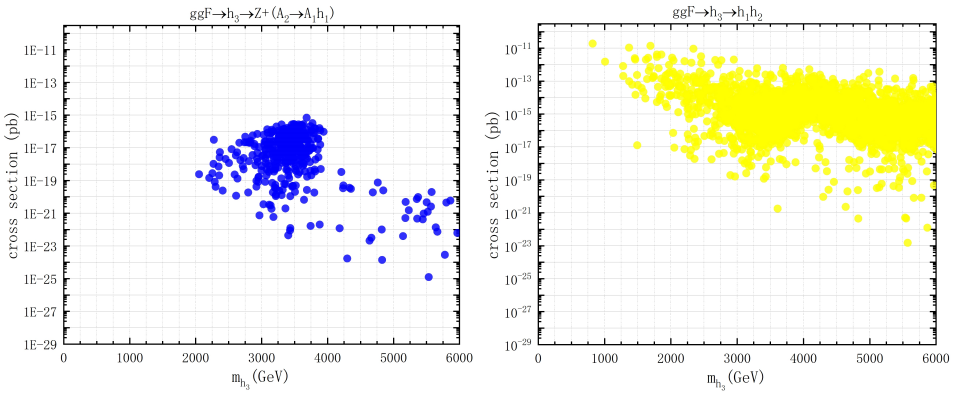


Figure 7. The cross-section of the heavy CP-even Higgs boson h_3 decaying into the SM-like Higgs boson at 13TeV LHC.

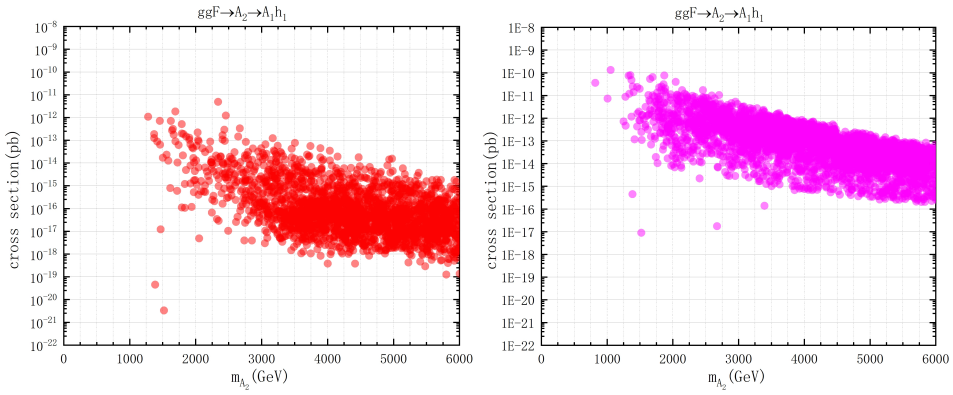


Figure 8. The cross-section of the heavy CP-odd Higgs boson A_2 decaying into the SM-like Higgs boson at 13 TeV LHC.

4. Summary

In this paper, we have performed phenomenological studies on the properties of dark matter and heavy Higgs bosons h_3 and A_2 in the μNMSSM. Considering the basic constraints from Higgs data, DM relic density, and LHC searches for sparticles, we have scanned the parameter space of the μNMSSM. We find that the LZ2022 experiment has a strict constraint on the parameter space of the μNMSSM, and the limits from the

DM-nucleon SI and SD cross-sections are complementary. Samples surviving the LZ2022 experiment and the muon anomaly constraint at the 2σ level are mainly featured by $\tan\beta \lesssim 20$, 850 GeV $\lesssim M_2 \lesssim$ 1500 GeV, and 100 GeV $\lesssim \mu_{\rm tot} \lesssim$ 300 GeV for Higgsino-dominated DM, or 100 GeV $\lesssim M_2 \lesssim$ 300 GeV, and 800 GeV $\lesssim \mu_{\rm tot} \lesssim$ 1000 GeV for Wino-dominated DM.

The detections of heavy Higgs bosons through exotic decay modes into SM-like Higgs bosons are important for analyzing the Higgs signals. We find that for doublet-dominated Higgs h_3, and A_2, the main exotic decay channels are $h_3 \to ZA_1$, $h_3 \to h_1h_2$, $A_2 \to A_1h_1$ and $A_2 \to Zh_2$, and the branching ratio can reach about 23%, 10%, 35%, and 10%, respectively. At the 13 TeV LHC, the production cross-section of processes $ggF \to h_3 \to h_1h_2$ and $ggF \to A_2 \to A_1h_1$ can reach to about 10^{-11} pb and 10^{-10} pb, respectively. This spectrum is hardly tested, but it is free from current constraints from the LHC on exotic Higgs. It is unfortunate that these heavy Higgs still cannot be tested at the High-Luminosity LHC (HL-LHC) [107]; one has to wait for the next-generation hadron colliders (such as the SPPC [108] and FCC-hh [109]) in order to investigate this parameter space.

Author Contributions: Conceptualization, Z.H. and L.S.; writing, Z.H. and X.L.; calculating, L.S. and X.L. All authors have read and agreed to the published version of the manuscript.

Funding: This work is supported by the China Scholarship Council under Grant No. 202208410277, and also by the High Performance Computing Center of Henan Normal University.

Data Availability Statement: Data is available upon a reasonable request to the authors.

Conflicts of Interest: The authors declare no conflicts of interest.

References

1. Aad, G. et al. [Atlas Collaboration] Combined search for the Standard Model Higgs boson using up to 4.9 fb^{-1} of pp collision data at $\sqrt{s} = 7$ TeV with the ATLAS detector at the LHC. *Phys. Lett. B* **2012**, *710*, 49–66. [CrossRef]
2. Chatrchyan, S. et al. [CMS Collaboration] Observation of a New Boson at a Mass of 125 GeV with the CMS Experiment at the LHC. *Phys. Lett. B* **2012**, *716*, 30–61. [CrossRef]
3. Chatrchyan, S. et al. [CMS Collaboration] Combined Results of Searches for the Standard Model Higgs Boson in pp Collisions at $\sqrt{s} = 7$ TeV. *Phys. Lett. B* **2012**, *710*, 26–48. [CrossRef]
4. Abi, B. et al. [(Muon $g-2$ Collaboration)] Measurement of the Positive Muon Anomalous Magnetic Moment to 0.46 ppm. *Phys. Rev. Lett.* **2021**, *126*, 141801. [CrossRef] [PubMed]
5. Bennett, G.W. et al. [(Muon $g-2$ Collaboration)] Final Report of the Muon E821 Anomalous Magnetic Moment Measurement at BNL. *Phys. Rev. D* **2006**, *73*, 072003. [CrossRef]
6. Franke, F.; Fraas, H. Mass bounds for the neutral Higgs bosons in the next-to-minimal supersymmetric standard model. *Phys. Lett. B* **1995**, *353*, 234–242. [CrossRef]
7. Szleper, M. Search for the NMSSM Higgs bosons at the photon collider. *Int. J. Mod. Phys. A* **2005**, *20*, 7404–7411. [CrossRef]
8. Ellwanger, U. Phenomenological Aspects of the Next-to-Minimal Supersymmetric Standard Model. *Nucl. Phys. B Proc. Suppl.* **2010**, *200–202*, 113–119. [CrossRef]
9. Franke, F.; Fraas, H. Neutralinos and Higgs bosons in the next-to-minimal supersymmetric standard model. *Int. J. Mod. Phys. A* **1997**, *12*, 479–534. [CrossRef]
10. Ellwanger, U.; Hugonie, C.; Teixeira, A.M. The Next-to-Minimal Supersymmetric Standard Model. *Phys. Rept.* **2010**, *496*, 1–77. [CrossRef]
11. Cao, J.; Li, F.; Lian, J.; Pan, Y.; Zhang, D. Impact of LHC probes of SUSY and recent measurement of $(g-2)_\mu$ on $\mathbb{Z}_3$-NMSSM. *Sci. China Phys. Mech. Astron.* **2022**, *65*, 291012. [CrossRef]
12. Cao, J.; Lian, J.; Pan, Y.; Zhang, D.; Zhu, P. Improved $(g-2)_\mu$ measurement and singlino dark matter in μ-term extended $\mathbb{Z}_3$-NMSSM. *J. High Energy Phys.* **2021**, *9*, 175. [CrossRef]
13. Zhou, H.; Cao, J.; Lian, J.; Zhang, D. Singlino-dominated dark matter in Z3-symmetric NMSSM. *Phys. Rev. D* **2021**, *104*, 015017. [CrossRef]
14. Cao, J.; Lian, J.; Pan, Y.; Yue, Y.; Zhang, D. Impact of recent $(g-2)_\mu$ measurement on the light CP-even Higgs scenario in general Next-to-Minimal Supersymmetric Standard Model. *J. High Energy Phys.* **2022**, *3*, 203. [CrossRef]

15. Cao, J.; Li, D.; Lian, J.; Yue, Y.; Zhou, H. Singlino-dominated dark matter in general NMSSM. *J. High Energy Phys.* **2021**, *6*, 176. [CrossRef]
16. Cao, J.; Jia, X.; Meng, L.; Yue, Y.; Zhang, D. Status of the singlino-dominated dark matter in general Next-to-Minimal Supersymmetric Standard Model. *J. High Energy Phys.* **2023**, *3*, 198. [CrossRef]
17. Lopez-Fogliani, D.E.; Munoz, C. Proposal for a Supersymmetric Standard Model. *Phys. Rev. Lett.* **2006**, *97*, 041801. [CrossRef]
18. Sirunyan, A.M. et al. [CMS Collaboration] Search for a heavy pseudoscalar boson decaying to a Z and a Higgs boson at $\sqrt{s} = 13$ TeV. *Eur. Phys. J. C* **2019**, *79*, 564. [CrossRef]
19. Aaboud, M. et al. [The ATLAS Collaboration] Search for heavy resonances decaying into a W or Z boson and a Higgs boson in final states with leptons and b-jets in 36 fb^{-1} of $\sqrt{s} = 13$ TeV pp collisions with the ATLAS detector. *J. High Energy Phys.* **2018**, *3*, 174. Erratum in *J. High Energy Phys.* **2018**, *11*, 51. [CrossRef]
20. Aad, G. et al. [The ATLAS Collaboration] Search for heavy resonances decaying into a Z or W boson and a Higgs boson in final states with leptons and b-jets in 139 fb^{-1} of pp collisions at $\sqrt{s} = 13$ TeV with the ATLAS detector. *J. High Energy Phys.* **2023**, *6*, 16. [CrossRef]
21. Khachatryan, V. et al. [CMS Collaboration] Search for a pseudoscalar boson decaying into a Z boson and the 125 GeV Higgs boson in $\ell^+\ell^- b\bar{b}$ final states. *Phys. Lett. B* **2015**, *748*, 221–243. [CrossRef]
22. Sirunyan, A.M. et al. [The CMS Collaboration] Search for a heavy pseudoscalar Higgs boson decaying into a 125 GeV Higgs boson and a Z boson in final states with two tau and two light leptons at $\sqrt{s} = 13$ TeV. *J. High Energy Phys.* **2020**, *3*, 65. [CrossRef]
23. Sirunyan, A.M. et al. [The CMS Collaboration] Search for new neutral Higgs bosons through the H$\rightarrow$ ZA $\rightarrow \ell^+\ell^-$b$\bar{\text{b}}$ process in pp collisions at $\sqrt{s} = 13$ TeV. *J. High Energy Phys.* **2020**, *3*, 55. [CrossRef]
24. Aad, G. et al. [ATLAS Collaboration] Search for a heavy Higgs boson decaying into a Z boson and another heavy Higgs boson in the $\ell\ell bb$ and $\ell\ell WW$ final states in pp collisions at $\sqrt{s} = 13$ TeV with the ATLAS detector. *Eur. Phys. J. C* **2021**, *81*, 396. [CrossRef]
25. Tumasyan, A. et al. [The CMS Collaboration] Search for a heavy Higgs boson decaying into two lighter Higgs bosons in the $\tau\tau$bb final state at 13 TeV. *J. High Energy Phys.* **2021**, *11*, 57. [CrossRef]
26. Ellwanger, U.; Hugonie, C. Benchmark planes for Higgs-to-Higgs decays in the NMSSM. *Eur. Phys. J. C* **2022**, *82*, 406. [CrossRef]
27. Kling, F.; Li, H.; Pyarelal, A.; Song, H.; Su, S. Exotic Higgs Decays in Type-II 2HDMs at the LHC and Future 100 TeV Hadron Colliders. *J. High Energy Phys.* **2019**, *6*, 31. [CrossRef]
28. Kling, F.; Li, H.; Li, S.; Pyarelal, A.; Song, H.; Su, S.; Su, W. Exotic Higgs Decays in the Type-II 2HDMs at Current and Future pp Colliders. *arXiv* **2022**, arXiv:2205.12198.
29. Abel, S.A. Destabilizing divergences in the NMSSM. *Nucl. Phys. B* **1996**, *480*, 55–72. [CrossRef]
30. Maniatis, M. The Next-to-Minimal Supersymmetric extension of the Standard Model reviewed. *Int. J. Mod. Phys. A* **2010**, *25*, 3505–3602. [CrossRef]
31. Panagiotakopoulos, C.; Tamvakis, K. Stabilized NMSSM without domain walls. *Phys. Lett. B* **1999**, *446*, 224–227. [CrossRef]
32. Ferrara, S.; Kallosh, R.; Linde, A.; Marrani, A.; Van Proeyen, A. Superconformal Symmetry, NMSSM, and Inflation. *Phys. Rev. D* **2011**, *83*, 025008. [CrossRef]
33. Hollik, W.G.; Liebler, S.; Moortgat-Pick, G.; Paßehr, S.; Weiglein, G. Phenomenology of the inflation-inspired NMSSM at the electroweak scale. *Eur. Phys. J. C* **2019**, *79*, 75. [CrossRef]
34. Hollik, W.G.; Li, C.; Moortgat-Pick, G.; Paasch, S. Phenomenology of a Supersymmetric Model Inspired by Inflation. *Eur. Phys. J. C* **2021**, *81*, 141. [CrossRef]
35. Kolda, C.F.; Pokorski, S.; Polonsky, N. Stabilized singlets in supergravity as a source of the mu-parameter. *Phys. Rev. Lett.* **1998**, *80*, 5263–5266. [CrossRef]
36. Miller, D.J.; Nevzorov, R.; Zerwas, P.M. The Higgs sector of the next-to-minimal supersymmetric standard model. *Nucl. Phys. B* **2004**, *681*, 3–30. [CrossRef]
37. Cao, J.J.; Heng, Z.X.; Yang, J.M.; Zhang, Y.M.; Zhu, J.Y. A SM-like Higgs near 125 GeV in low energy SUSY: A comparative study for MSSM and NMSSM. *J. High Energy Phys.* **2012**, *3*, 86. [CrossRef]
38. King, S.F.; Mühlleitner, M.; Nevzorov, R.; Walz, K. Natural NMSSM Higgs Bosons. *Nucl. Phys. B* **2013**, *870*, 323–352. [CrossRef]
39. Wang, F.; Wang, W.; Wu, L.; Yang, J.M.; Zhang, M. Probing degenerate heavy Higgs bosons in NMSSM with vector-like particles. *Int. J. Mod. Phys. A* **2017**, *32*, 1745005. [CrossRef]
40. Aoyama, T.; Asmussen, N.; Benayoun, M.; Bijnens, J.; Blum, T.; Bruno, M.; Caprini, I.; Calame, C.C. Cè, M.; Colangelo, G.; et al. The anomalous magnetic moment of the muon in the Standard Model. *Phys. Rept.* **2020**, *887*, 1–166. [CrossRef]
41. Aoyama, T.; Hayakawa, M.; Kinoshita, T.; Nio, M. Complete Tenth-Order QED Contribution to the Muon g-2. *Phys. Rev. Lett.* **2012**, *109*, 111808. [CrossRef] [PubMed]
42. Aoyama, T.; Kinoshita, T.; Nio, M. Theory of the Anomalous Magnetic Moment of the Electron. *Atoms* **2019**, *7*, 28. [CrossRef]
43. Czarnecki, A.; Marciano, W.J.; Vainshtein, A. Refinements in electroweak contributions to the muon anomalous magnetic moment. *Phys. Rev. D* **2003**, *67*, 073006; Erratum in *Phys. Rev. D* **2006**, *73*, 119901. [CrossRef]

44. Gnendiger, C.; Stöckinger, D.; Stöckinger-Kim, H. The electroweak contributions to $(g-2)_\mu$ after the Higgs boson mass measurement. *Phys. Rev. D* **2013**, *88*, 053005. [CrossRef]
45. Keshavarzi, A.; Nomura, D.; Teubner, T. Muon $g-2$ and $\alpha(M_Z^2)$: A new data-based analysis. *Phys. Rev. D* **2018**, *97*, 114025. [CrossRef]
46. Stoffer, P.; Colangelo, G.; Hoferichter, M. Two-pion contributions to the muon g – 2. *PoS* **2019**, *CD2018*, 84. [CrossRef]
47. Colangelo, G.; Hoferichter, M.; Stoffer, P. Two-pion contribution to hadronic vacuum polarization. *J. High Energy Phys.* **2019**, *2*, 6. [CrossRef]
48. Davier, M.; Hoecker, A.; Malaescu, B.; Zhang, Z. Reevaluation of the hadronic vacuum polarisation contributions to the Standard Model predictions of the muon $g-2$ and $\alpha(m_Z^2)$ using newest hadronic cross-section data. *Eur. Phys. J. C* **2017**, *77*, 827. [CrossRef]
49. Keshavarzi, A.; Nomura, D.; Teubner, T. $g-2$ of charged leptons, $\alpha(M_Z^2)$, and the hyperfine splitting of muonium. *Phys. Rev. D* **2020**, *101*, 014029. [CrossRef]
50. Hoferichter, M.; Hoid, B.L.; Kubis, B. Three-pion contribution to hadronic vacuum polarization. *J. High Energy Phys.* **2019**, *8*, 137. [CrossRef]
51. Kurz, A.; Liu, T.; Marquard, P.; Steinhauser, M. Hadronic contribution to the muon anomalous magnetic moment to next-to-next-to-leading order. *Phys. Lett. B* **2014**, *734*, 144–147. [CrossRef]
52. Melnikov, K.; Vainshtein, A. Hadronic light-by-light scattering contribution to the muon anomalous magnetic moment revisited. *Phys. Rev. D* **2004**, *70*, 113006. [CrossRef]
53. Masjuan, P.; Sanchez-Puertas, P. Pseudoscalar-pole contribution to the $(g_\mu-2)$: A rational approach. *Phys. Rev. D* **2017**, *95*, 054026. [CrossRef]
54. Hoferichter, M.; Hoid, B.L.; Kubis, B.; Leupold, S.; Schneider, S.P. Dispersion relation for hadronic light-by-light scattering: Pion pole. *J. High Energy Phys.* **2018**, *10*, 141. [CrossRef]
55. Gérardin, A.; Meyer, H.B.; Nyffeler, A. Lattice calculation of the pion transition form factor with $N_f = 2+1$ Wilson quarks. *Phys. Rev. D* **2019**, *100*, 034520. [CrossRef]
56. Colangelo, G.; Hagelstein, F.; Hoferichter, M.; Laub, L.; Stoffer, P. Longitudinal short-distance constraints for the hadronic light-by-light contribution to $(g-2)_\mu$ with large-N_c Regge models. *J. High Energy Phys.* **2020**, *3*, 101. [CrossRef]
57. Blum, T.; Chowdhury, S.; Hayakawa, M.; Izubuchi, T. Hadronic light-by-light scattering contribution to the muon anomalous magnetic moment from lattice QCD. *Phys. Rev. Lett.* **2015**, *114*, 012001. [CrossRef]
58. Boccaletti, A.; Borsanyi, S.; Davier, M.; Fodor, Z.; Frech, F.; Gerardin, A.; Giusti, D.; Kotov, A.Y.; Lellouch, L.; Lippert, T.; et al. High precision calculation of the hadronic vacuum polarisation contribution to the muon anomaly. *arXiv* **2024**, arXiv:2407.10913.
59. Aguillard, D.P. et al. [The Muon $g-2$ Collaboration] Measurement of the Positive Muon Anomalous Magnetic Moment to 0.20 ppm. *Phys. Rev. Lett.* **2023**, *131*, 161802. [CrossRef]
60. Hunt-Smith, N.T.; Melnitchouk, W.; Sato, N.; Thomas, A.W.; Wang, X.G.; White, M.J. Global QCD analysis and dark photons. *J. High Energy Phys.* **2023**, *9*, 96. [CrossRef]
61. Li, S.; Xiao, Y.; Yang, J.M. Constraining CP-phases in SUSY: An interplay of muon/electron g-2 and electron EDM. *Nucl. Phys. B* **2022**, *974*, 115629. [CrossRef]
62. Li, Z.; Liu, G.L.; Wang, F.; Yang, J.M.; Zhang, Y. Gluino-SUGRA scenarios in light of FNAL muon g $-$ 2 anomaly. *J. High Energy Phys.* **2021**, *12*, 219. [CrossRef]
63. Du, X.; Wang, F. NMSSM from Alternative Deflection in Generalized Deflected Anomaly Mediated SUSY Breaking. *Eur. Phys. J. C* **2018**, *78*, 431. [CrossRef]
64. Wang, K.; Wang, F.; Zhu, J.; Jie, Q. The semi-constrained NMSSM in light of muon g-2, LHC, and dark matter constraints. *Chin. Phys. C* **2018**, *42*, 103109. [CrossRef]
65. Cox, P.; Han, C.; Yanagida, T.T. Muon $g-2$ and dark matter in the minimal supersymmetric standard model. *Phys. Rev. D* **2018**, *98*, 055015. [CrossRef]
66. Yang, J.L.; Feng, T.F.; Yan, Y.L.; Li, W.; Zhao, S.M.; Zhang, H.B. Lepton-flavor violation and two loop electroweak corrections to $(g-2)_\mu$ in the B-L symmetric SSM. *Phys. Rev. D* **2019**, *99*, 015002. [CrossRef]
67. Li, S.; Xiao, Y.; Yang, J.M. Can electron and muon $g-2$ anomalies be jointly explained in SUSY? *Eur. Phys. J. C* **2022**, *82*, 276. [CrossRef]
68. Wang, F.; Wu, L.; Xiao, Y.; Yang, J.M.; Zhang, Y. GUT-scale constrained SUSY in light of new muon g-2 measurement. *Nucl. Phys. B* **2021**, *970*, 115486. [CrossRef]
69. Aboubrahim, A.; Klasen, M.; Nath, P.; Syed, R.M. Tests of gluino-driven radiative breaking of the electroweak symmetry at the LHC. *Phys. Scr.* **2022**, *97*, 054002. [CrossRef]
70. Wang, K.; Zhu, J. Smuon in the NMSSM confronted with the muon g–2 anomaly and SUSY searches. *Chin. Phys. C* **2023**, *47*, 013107. [CrossRef]
71. Zheng, M.D.; Zhang, H.H. Studying the $b \to s\ell^+\ell^-$ anomalies and $(g-2)_\mu$ in R-parity violating MSSM framework with the inverse seesaw mechanism. *Phys. Rev. D* **2021**, *104*, 115023. [CrossRef]

72. Domingo, F.; Ellwanger, U. Constraints from the Muon g-2 on the Parameter Space of the NMSSM. *J. High Energy Phys.* **2008**, *7*, 79. [CrossRef]
73. Athron, P.; Bach, M.; Fargnoli, H.G.; Gnendiger, C.; Greifenhagen, R.; Park, J.h.; Paßehr, S.; Stöckinger, D.; Stöckinger-Kim, H.; Voigt, A. GM2Calc: Precise MSSM prediction for $(g-2)$ of the muon. *Eur. Phys. J. C* **2016**, *76*, 62. [CrossRef]
74. Endo, M.; Hamaguchi, K.; Iwamoto, S.; Kitahara, T. Supersymmetric interpretation of the muon g − 2 anomaly. *J. High Energy Phys.* **2021**, *7*, 75. [CrossRef]
75. Almarashi, M.M.; Alhazmi, F.; Abdulhafidh, R.; Basir, S.A. Dark matter in NMSSM with small λ and κ. *Results Phys.* **2023**, *49*, 106531. [CrossRef]
76. Wang, L.; Yang, J.M.; Zhang, Y.; Zhu, P.; Zhu, R. A Concise Review on Some Higgs-Related New Physics Models in Light of Current Experiments. *Universe* **2023**, *9*, 178. [CrossRef]
77. Badziak, M.; Olechowski, M.; Szczerbiak, P. Blind spots for neutralino dark matter in the NMSSM. *J. High Energy Phys.* **2016**, *3*, 179. [CrossRef]
78. Badziak, M.; Olechowski, M.; Szczerbiak, P. Spin-dependent constraints on blind spots for thermal singlino-higgsino dark matter with(out) light singlets. *J. High Energy Phys.* **2017**, *7*, 50. [CrossRef]
79. Badziak, M.; Olechowski, M.; Szczerbiak, P. Blind spots for neutralinos in NMSSM with light singlet scalar. *PoS* **2015**, *PLANCK2015*, 130.
80. Pierce, A.; Shah, N.R.; Freese, K. Neutralino Dark Matter with Light Staus. *arXiv* **2013**, arXiv:1309.7351.
81. Shang, L.; Zhang, Y. EasyScan_HEP: A tool for connecting programs to scan the parameter space of physics models. *arXiv* **2023**, arXiv:2304.03636.
82. Staub, F. SARAH. *arXiv* **2008**, arXiv:0806.0538.
83. Staub, F. SARAH 3.2: Dirac Gauginos, UFO output, and more. *Comput. Phys. Commun.* **2013**, *184*, 1792–1809. [CrossRef]
84. Staub, F. SARAH 4: A tool for (not only SUSY) model builders. *Comput. Phys. Commun.* **2014**, *185*, 1773–1790. [CrossRef]
85. Staub, F. Exploring new models in all detail with SARAH. *Adv. High Energy Phys.* **2015**, *2015*, 840780. [CrossRef]
86. Porod, W. SPheno, a program for calculating supersymmetric spectra, SUSY particle decays and SUSY particle production at e+ e- colliders. *Comput. Phys. Commun.* **2003**, *153*, 275–315. [CrossRef]
87. Porod, W.; Staub, F. SPheno 3.1: Extensions including flavour, CP-phases and models beyond the MSSM. *Comput. Phys. Commun.* **2012**, *183*, 2458–2469. [CrossRef]
88. Bélanger, G.; Boudjema, F.; Pukhov, A.; Semenov, A. micrOMEGAs4.1: Two dark matter candidates. *Comput. Phys. Commun.* **2015**, *192*, 322–329. [CrossRef]
89. Belanger, G.; Boudjema, F.; Pukhov, A.; Semenov, A. MicrOMEGAs: A Program for calculating the relic density in the MSSM. *Comput. Phys. Commun.* **2002**, *149*, 103–120. [CrossRef]
90. Belanger, G.; Boudjema, F.; Pukhov, A.; Semenov, A. micrOMEGAs_3: A program for calculating dark matter observables. *Comput. Phys. Commun.* **2014**, *185*, 960–985. [CrossRef]
91. Belanger, G.; Boudjema, F.; Pukhov, A.; Semenov, A. micrOMEGAs: A Tool for dark matter studies. *Nuovo Cim. C* **2010**, *033N2*, 111–116. [CrossRef]
92. Belanger, G.; Boudjema, F.; Brun, P.; Pukhov, A.; Rosier-Lees, S.; Salati, P.; Semenov, A. Indirect search for dark matter with micrOMEGAs2.4. *Comput. Phys. Commun.* **2011**, *182*, 842–856. [CrossRef]
93. Belanger, G.; Boudjema, F.; Pukhov, A.; Semenov, A. Dark matter direct detection rate in a generic model with micrOMEGAs 2.2. *Comput. Phys. Commun.* **2009**, *180*, 747–767. [CrossRef]
94. Belanger, G.; Boudjema, F.; Pukhov, A.; Semenov, A. micrOMEGAs 2.0.7: A program to calculate the relic density of dark matter in a generic model. *Comput. Phys. Commun.* **2007**, *177*, 894–895. [CrossRef]
95. Belanger, G.; Boudjema, F.; Pukhov, A.; Semenov, A. MicrOMEGAs 2.0: A Program to calculate the relic density of dark matter in a generic model. *Comput. Phys. Commun.* **2007**, *176*, 367–382. [CrossRef]
96. Belanger, G.; Boudjema, F.; Pukhov, A.; Semenov, A. micrOMEGAs: Version 1.3. *Comput. Phys. Commun.* **2006**, *174*, 577–604. [CrossRef]
97. Belanger, G.; Boudjema, F.; Pukhov, A.; Semenov, A. micrOMEGAs: Recent developments. In Proceedings of the 4th International Workshop on the Identification of Dark Matter, York, UK, 2–6 September 2002; pp. 262–267. [CrossRef]
98. Bechtle, P.; Heinemeyer, S.; Stål, O.; Stefaniak, T.; Weiglein, G. Probing the Standard Model with Higgs signal rates from the Tevatron, the LHC and a future ILC. *J. High Energy Phys.* **2014**, *11*, 39. [CrossRef]
99. Bechtle, P.; Heinemeyer, S.; Stal, O.; Stefaniak, T.; Weiglein, G. Applying Exclusion Likelihoods from LHC Searches to Extended Higgs Sectors. *Eur. Phys. J. C* **2015**, *75*, 421. [CrossRef]
100. Bagnaschi, E.; Sakurai, K.; Borsato, M.; Buchmueller, O.; Citron, M.; Costa, J.C.; De Roeck, A.; Dolan, M.J.; Ellis, J.R.; Flächer, H.; et al. Likelihood Analysis of the pMSSM11 in Light of LHC 13-TeV Data. *Eur. Phys. J. C* **2018**, *78*, 256. [CrossRef]
101. Khosa, C.K.; Kraml, S.; Lessa, A.; Neuhuber, P.; Waltenberger, W. SModelS Database Update v1.2.3. *J. High Energy Phys.* **2020**, *2020*, 158. [CrossRef]

102. Mahdi Altakach, M.; Kraml, S.; Lessa, A.; Narasimha, S.; Pascal, T.; Waltenberger, W. SModelS v2.3: Enabling global likelihood analyses. *arXiv* **2023**, arXiv:2306.17676.
103. Dutta, J.; Kraml, S.; Lessa, A.; Waltenberger, W. SModelS extension with the CMS supersymmetry search results from Run 2. *J. High Energy Phys.* **2018**, *1*, 5–12. [CrossRef]
104. Ambrogi, F.; Dutta, J.; Heisig, J.; Kraml, S.; Kulkarni, S.; Laa, U.; Lessa, A.; Neuhuber, P.; Reyes-González, H.; Waltenberger, W.; et al. SModelS v1.2: Long-lived particles, combination of signal regions, and other novelties. *Comput. Phys. Commun.* **2020**, *251*, 106848. [CrossRef]
105. Beenakker, W.; Hopker, R.; Spira, M. PROSPINO: A Program for the production of supersymmetric particles in next-to-leading order QCD. *arXiv* **1996**, arXiv:hep-ph/9611232.
106. Aalbers, J. et al. [LUX-ZEPLIN Collaboration] First Dark Matter Search Results from the LUX-ZEPLIN (LZ) Experiment. *Phys. Rev. Lett.* **2023**, *131*, 041002. [CrossRef] [PubMed]
107. Aberle, O.; Adorisio, C.; Adraktas, A.; Ady, M.; Albertone, J.; Alberty, L.; Alcaide Leon, M.; Alekou, A.; Alesini, D.; Almeida Ferreira, B.; et al. *High-Luminosity Large Hadron Collider (HL-LHC): Technical Design Report*; CERN: Geneva, Switzerland , 2020; Volume 10. [CrossRef]
108. CEPC Study Group. CEPC Conceptual Design Report: Volume 1—Accelerator. *arXiv* **2018**, arXiv:1809.00285.
109. Abada, A. et al. [The FCC Collaboration] FCC-hh: The Hadron Collider: Future Circular Collider Conceptual Design Report Volume 3. *Eur. Phys. J. Spec. Top.* **2019**, *228*, 755–1107. [CrossRef]

Disclaimer/Publisher's Note: The statements, opinions and data contained in all publications are solely those of the individual author(s) and contributor(s) and not of MDPI and/or the editor(s). MDPI and/or the editor(s) disclaim responsibility for any injury to people or property resulting from any ideas, methods, instructions or products referred to in the content.